minerals

MDPI

Article

Late Devonian A-Type Granites from the Beishan, Southern Central Asia Orogenic Belt: Implications for Closure of the Paleo-Asia Ocean

Erteng Wang, Xinwei Zhai *, Wanfeng Chen, Lei Wu, Gaorui Song, Yun Wang, Zhiang Guo, Jiaolong Zhao and Jinrong Wang

Key Laboratory of Mineral Resources in Western China (Gansu Province), School of Earth Sciences, Lanzhou University, Lanzhou 730000, China; wanget19@lzu.edu.cn (E.W.)
* Correspondence: zhaixw926@lzu.edu.cn

Abstract: The closing time of the Paleo-Asian Ocean (PAO) has long been in the focus of research as well as of controversial debates. The Paleozoic A-type granites distributed in the Beishan Orogenic Belt (BOB) at the southern margin of the Central Asian Orogenic Belt (CAOB) provide pivotal clues to constrain the closure of the PAO. In this paper, the newly recognized Duhongshan A-type granites from the middle Huaniushan arc in the BOB (zircon LA-ICP-MS U-Pb ages of ca. 376–374 Ma) are thoroughly studied. The rocks have high SiO_2, K_2O contents with peralkaline character, and display high Zr + Nb + Ce + Y contents (354–543 ppm), 10,000 × Ga/Al (4.1–4.9), Y/Nb (3.2–5.3), Rb/Nb ratios (8.5–14.1), and a zircon saturation temperature in the range of 877–950 °C, indicative of A2-type granites affinities. The Duhongshan granites display enriched in Th and U; depleted in Ba, Sr, and Ti; with slightly positive whole-rock $\varepsilon_{Nd}(t)$ values (+1.86 to +2.21), indicating an origin related to partial melting of lower crustal material in post-collision extension settings. Combined with previous reported results, we conclude that the granitoids in the middle Huaniushan arc were mostly formed around 424–367 Ma and can be divided into two types based on petrochemistry: (a) A-type granites, which generally have high SiO_2 and K_2O, derived from the relatively shallow crustal source in post-collision tectonic settings; and (b) adakite and I-type granites, which display high Sr/Y ratios as well as Nb, Ta, and Ti depletion, likely generated from the melting of juvenile crust in active continental margin arcs. Integrating the previous regional investigations, we propose that the Hongliuhe–Niujuanzi–Xichangjing Ocean (HNXO) of the PAO was closed and transformed in the post-collision extensional tectonic stage during the Late Devonian and formed as post-collision magmatism, while the arc magmatism may be related to the subduction of the Liuyuan Ocean, which is located in the Southern HNXO.

Keywords: a-type granite; Late Devonian; Beishan; closure of the Paleo-Asian Ocean; Central Asia Orogenic Belt

Citation: Wang, E.; Zhai, X.; Chen, W.; Wu, L.; Song, G.; Wang, Y.; Guo, Z.; Zhao, J.; Wang, J. Late Devonian A-Type Granites from the Beishan, Southern Central Asia Orogenic Belt: Implications for Closure of the Paleo-Asia Ocean. *Minerals* **2023**, *13*, 565. https://doi.org/10.3390/min13040565

Academic Editor: Simon Paul Johnson

Received: 6 March 2023
Revised: 7 April 2023
Accepted: 13 April 2023
Published: 18 April 2023

1. Introduction

The Central Asian Orogenic Belt (CAOB) is a vast Phanerozoic accretive orogenic belt, which is located along the Southern Siberian Craton, Eastern Baltica Craton, Northern North China Craton and Tarim Craton (Figure 1a). When the Paleo-Asian Ocean (PAO) subducted and closed during the Paleozoic, the CAOB was formed by a collage of seamounts, island arcs, microcontinents, and ophiolites [1–5]. Although numerous studies over the past decade have suggested that the southern margin of the CAOB is the final location of the closure of the PAO [6–14], the timing of the final closure of the PAO has been one of the most controversial issues. Fortunately, there exists a large number of different types of granites (I-, S-and A-type granites, adakite, etc.) associated with accretive orogenesis and oceanic subduction in the Southern CAOB [14–19], which is valuable utility to study for the subduction–collision history of the PAO and the formation of the CAOB.

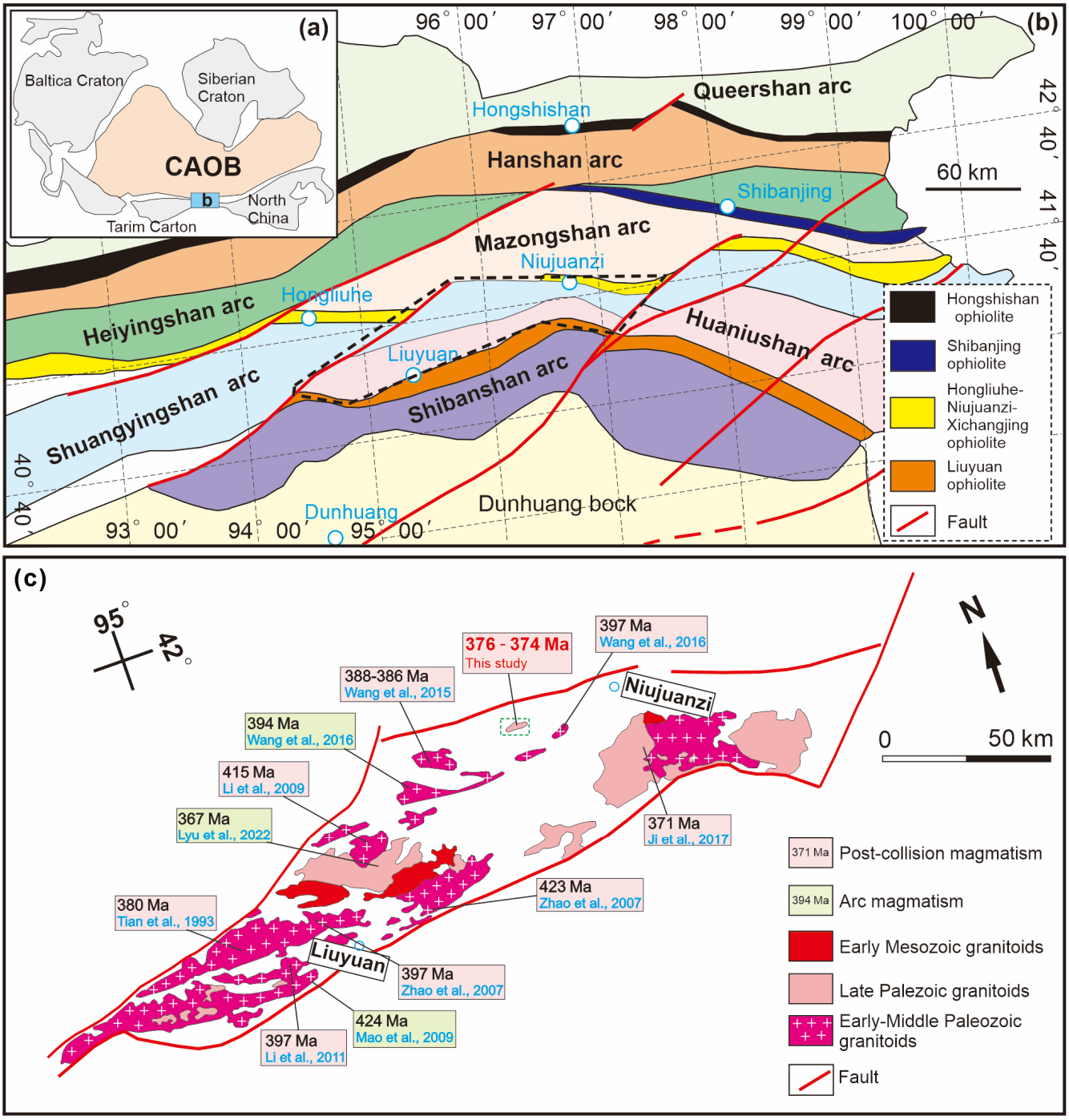

Figure 1. (**a**) Simplified tectonic map of the Central Asian Orogenic Belt showing the location of the Bieshan Orogenic Belt (BOB) [20]. (**b**) Tectonic divisions map of the BOB [20]. (**c**) Distribution of Paleozoic granitoids in the middle Huaniushan arc (modified after [21]). Figure 1c shows early Paleozoic felsic magmatism in the middle of the Huaniushan arc. The post-collision magmatism has produced A-type granites, and the arc magmatism is mostly I-type granites and adakite (age data from [15,18,22–28]).

The Beishan Orogenic Belt (BOB) is a major part of the middle Southern CAOB (Figure 1a), as well as an important branch ocean of the PAO [20,21,29]. Four major branch oceans (as seen in Figure 1b; their former existence is evidenced by the Hongshishan ophiolite, Mingshui–Xiaohuangshan ophiolite, Hongliuhe–Niujuanzi-Xichangjing ophiolite, and Liuyuan ophiolite) and relative island arcs (Figure 1b) developed in the BOB over a

long period of ocean–continental tectonic evolution during the Paleozoic, demonstrating a multi-island arc–ocean tectonic evolution framework. Some scholars have proposed that the ocean began its subduction during the Early Paleozoic [30–33], and that all of the branch oceans had closed during the Permian–Triassic period [19–21,32,34], influenced by the later superimposed reformation. However, other investigators conclude that the different branch oceans of the BOB closed one after the other from the Devonian to the Triassic [13,30,35–38]. Specifically, the Hongliuhe–Niujuanzi–Xichangjing Ocean (HNXO) (Figure 1b), the major branch ocean of the PAO in the BOB, is the earliest ocean that closed [29,30,32,39]. Thus, the closing time of the HNXO is crucial to understand the tectonic evolution of the BOB during the Paleozoic. At present, there are different opinions on the closure time of the HNXO, e.g., Middle–Late Silurian or Late Devonian [11,37]. The disputes are ascribed to incomplete knowledge on the tectonic events that happened during ocean accretion, closure, and post-orogenesis in the BOB [37,40]. As a result, there is not enough reliable geological evidence to constraint the closure time of the ocean.

Most of the A-type granites in the Southern CAOB were developed during the post-collision extensional tectonic setting after the closing of the PAO [19,41,42], and offer reliable petrological and geochronological information to effectively identify the closure time of the ocean. In this paper, we present zircon U-Pb isotope as well as whole-rock major- and trace-element and Nd isotope data for the Duhongshan A-type granite from the Huaniushan arc in the Southern BOB to reveal its origin and tectonic setting, combining this with regional geological events to define the HNXO's closure time. The new results are particularly important to further study the tectonic evolution of the CAOB.

2. Geological Background and Description of Samples

2.1. Geological Background

The BOB is located in the Southern CAOB and the Northern Dunhuang Block (Figure 1b) and is made up by a few Mesoproterozoic to Neoproterozoic microcontinents, Paleozoic felsic–mafic magmatic and volcaniclastic rocks, sedimentary stratal, and ophiolitic mélanges [11,15,17,20,29,43–46]. From north to south, four major ophiolite belts (Hongshishan ophiolites, Mingshui–Xiaohuangshan ophiolites, Hongliuhe-Niujuanzi-Xichangjing ophiolites, and Liuyuan ophiolites) divide the BOB into the Queershan arc, Hanshan arc (Hanshan–Heiyingshan arc), Mazongshan arc, Huaniushan arc (Huaniushan–Shuangyingshan arc), and Shibanshan arc (Figure 1b) [20].

This research focuses on the middle Huaniushan arc, situated between the Niujuanzi ophiolite belt to the south and the Liuyuan ophiolite belt to the north (Figure 1b). The Huaniushan arc was generated by the subduction of the HNXO in the Early Paleozoic, which may be similar for the Japanese-type island arc [15,20,47]. The Huaniushan arc most likely has a Precambrian basement as indicated by the granitic g neiss (902–870 Ma) found in Liuyuan [48–51]. The Paleozoic to the Mesozoic in the middle of the Huaniushan arc are felsic intrusive rocks, e.g., granites, monzogranites, syenogranites, and granodiorites (Figure 1c). Additionally, a small amount of mafic igneous rocks are also distributed in the Huaniushan arc [52]. The Neoproterozoic marble and dolomite are found in Shuangyingshan. Most of the Cambrian–Ordovician strata are located in the Niujuanzi area. The Cambrian is mostly composed of thin layers of limestone and micritic limestone, suggesting a shallow to semi-deep-sea environment. The Ordovician is a flysch formation interbedded with feldspar-bearing sandstone. The Silurian is a volcanic flysch formation composed of volcanic, volcaniclastic, and sedimentary clastic rocks. The Devonian includes limestone, sandstone, and andesite, which are only found in the Huaniushan arc [29,31,53,54]. The Carboniferous–Permian is mainly composed of basaltic to felsic volcanic rocks, carbonate and clastic sedimentary rocks in the Shibanshan arc [20,48,54–56].

2.2. Description of Samples

The Duhongshan pluton addressed in this paper is located on the Northern Huaniushan arc (Figure 1c), covering an area of around 30 km^2. It is mostly composed of

monzogranite and intrudes into the Ordovician siliceous rocks. Two samples (DSH11 and DSH15) were collected for geochronological studies and fourteen samples for geochemical investigations (Figure 2). The Duhongshan granite is of light flesh-red color, medium- and coarse-grained and has a massive structure (Figure 3a,b). The samples consist mainly of the quartz (45 vol%), K-feldspar (25 vol%), plagioclase (20 vol%), biotite (~5 vol%), and a small amount of amphibole (<5 vol%) (Figure 3c). The K-feldspar and plagioclase grains are euhedral clinopyroxene. The biotite and amphibole from irregular crystals, filling in the spaces between the grains of quartz and feldspar showing late recrystallization (Figure 3c,d).

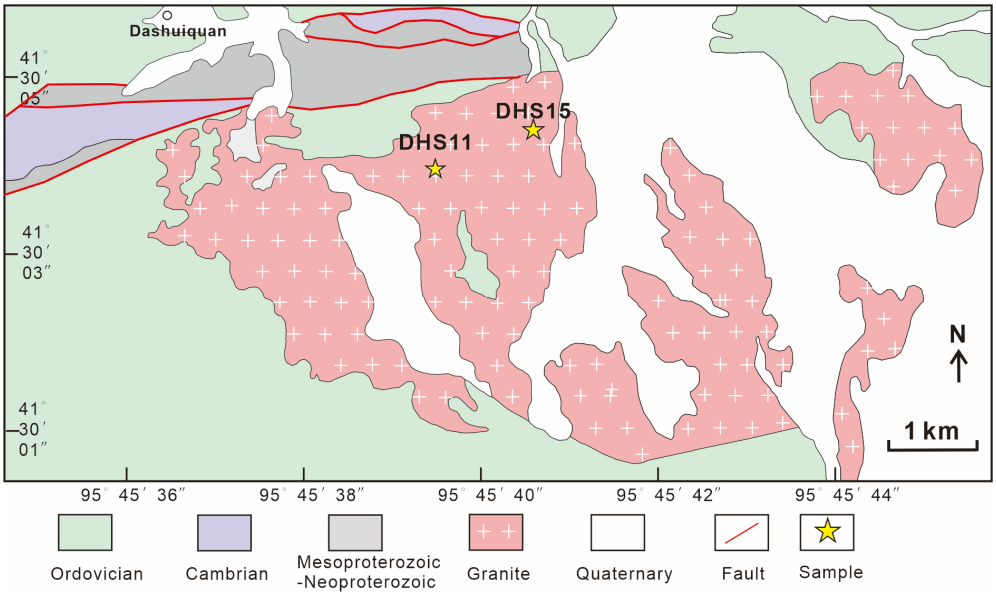

Figure 2. Geological map of the study area in the middle Huaniushan arc (modified from 1: 50,000 geological maps of the Duhongshan area).

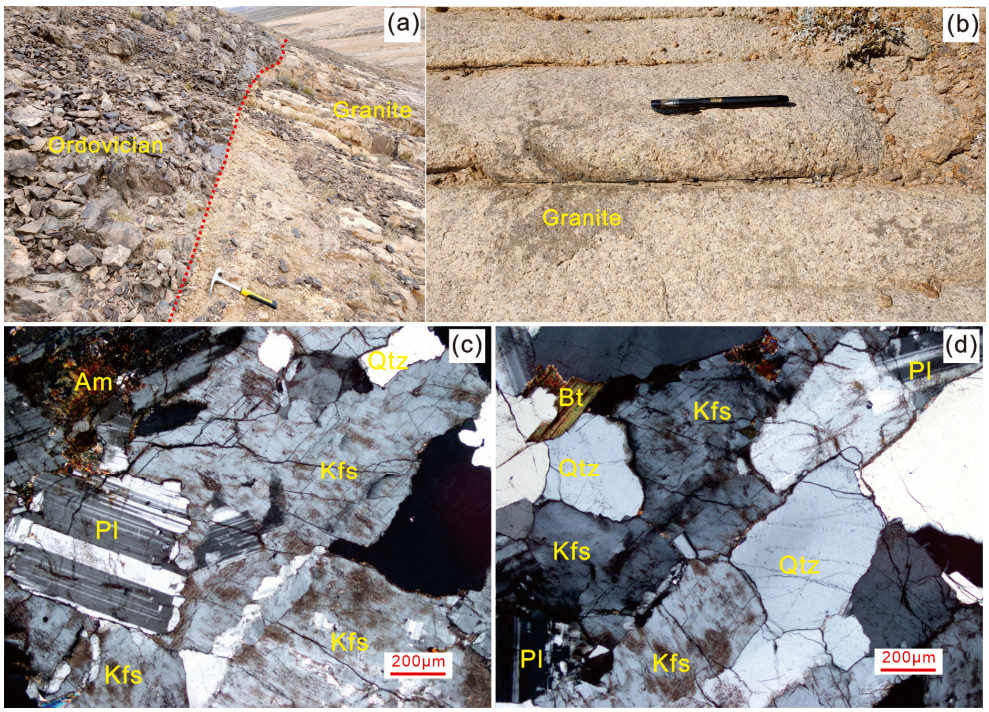

Figure 3. Representative field photographs (**a**,**b**) and photomicrographs (**c**,**d**) of the Late Devonian Duhongshan granites. The granite intrudes into the Ordovician silica rock in the Figure 3a. Mineral abbreviations: Qtz = quartz; Kfs = K-feldspar; Pl = plagioclase; Bt = biotite; Am = amphibole.

3. Analytical Methods

Zircon U-Pb dating and whole-rock geochemistry were performed at the Key Laboratory of Mineral Resources in Western China (Gansu Province), Lanzhou University. Whole-rock Nd isotope measurements were carried out at Nanjing Hongchuang Geological Exploration Technology Service Co., Ltd., Nanjing, China.

3.1. Zircon U-Pb Dating

Heavy liquid and magnetic methods were employed to separate the zircon grains from the 5 kg samples. They were selected, placed on epoxy resin discs, polished to half their thickness, coated with carbon, and photographed under reflected and transmitted light. The Mono CL3 Cathodoluminescence (CL) System was used to acquire high-resolution CL pictures. The U-Pb isotope ratios of the selected zircons were measured using an Agilent 7500X ICP-MS instrument combined with a Geo-Las200M laser ablation (LA) system. During the test, 91,500 and NIST610 standard samples were used as the external standard and element content, respectively, and Si was used as the internal standard element. The GLITTER4.4 and ISOPLOT3.0 software were employed to process the data.

3.2. Whole-Rock Major and Trace Element Analyes

First, the studied samples rock were mechanically crushed and ground to 200 mesh. The BLi_3O_3 alkali melting procedure was employed in this work to decompose the rock powders prior to the main element test. ICP optical emission spectroscopy (ICP-OES) was used to evaluate the compositions of the main elements. The analytical precision was better than 2%. About 0.5 g of dry sample powder was heated at 1000 °C for two hours to achieve loss on ignition (LOI). ICP-MS was used for trace elements analysis, and the Agilent 7700 instrument's analytical errors were less than 10%. The standards were based on the US Geological Survey reference documents AGV-2 and BCR-2.

3.3. Whole-Rock Nd Isotope Analyses

The Nd-bearing elution was gently evaporated to dryness and re-dissolved in 1.0 mL 2 wt.% HNO_3. Small aliquots of each sample were analyzed for exact elements concentration by Agilent Technologies 7700 quadrupole ICP-MS (Hachioji, Tokyo, Japan). A diluted solution (50 ppb Nd) was introduced into Nu Instruments Nu Plasma II MC-ICP-MS (Wrexham, Wales, UK) through the Teledyne Cetac Technologies Aridus II Desolvating Nebulizer System (Omaha, NE, USA). Raw data of Nd isotopic ratios were internally corrected for mass fractionation by normalizing to $^{146}Nd/^{144}Nd = 0.7219$ with the exponential law. The international isotopic standard JNdi-1 was periodically analyzed to correct instrumental drift. The geochemical reference materials of USGS RGM-2 were treated as quality control. These Nd isotopic results agree with previous publications within analytical uncertainty [50].

4. Analytical Results

The zircon U-Pb isotopes and trace elements data, whole-rock major and trace elements data and whole-rock Nd isotope data for the Duhongshan granites are listed in Supplementary Tables S1–S4.

4.1. Zircon U-Pb Geochronology

The samples DSH11 and DSH15 were collected from medium-grained and medium-to-fine grained monzogranite of the Duhongshan pluton, respectively. Concordia diagrams and representative CL images of the analyzed zircon grains are shown in Figure 4. The zircon grains from the sample DSH11 are short prismatic with a length ranging from 50 to 180 μm and a width ranging from 50 to 100 μm. They displayed a relative dark color in the CL image with a high content of U (Table S2), which indicates a U-rich zircon [57]. As seen in Figure 5, they display positive Ce and large negative Eu anomalies [58,59]. In addition, the zircon grains have high Th/U ratios (0.52–1.79). These features indicate a

zircon of magmatic origin. Sixteen zircon grains yielded concordant $^{206}Pb/^{238}U$ ratios with a weighted mean $^{206}Pb/^{238}U$ age of 376 ± 2.1 Ma (MSWD = 1.06; n = 15), interpreted as the crystallization age of the DSH11 sample (Figure 4). The zircon grains from the DSH15 sample are columnar with a length ranging from 100 to 200 µm and a width ranging from 60 to 80 µm. They are also U-rich (Table S2) and displayed characteristics of magmatic origin, namely high Th/U ratios (0.31–0.79) with positive Ce and large negative Eu anomalies (Figure 5). Fourteen zircon grains have concordant $^{206}Pb/^{238}U$ ratios with a weighted mean $^{206}Pb/^{238}U$ age of 374.7 ± 2.4 Ma (MSWD = 1.08; n = 14), interpreted as the crystallization age of the DSH15 sample (Figure 4). This age, together with the age of the DHS11 sample, suggested that the Duhongshan pluton was formed in the Late Devonian.

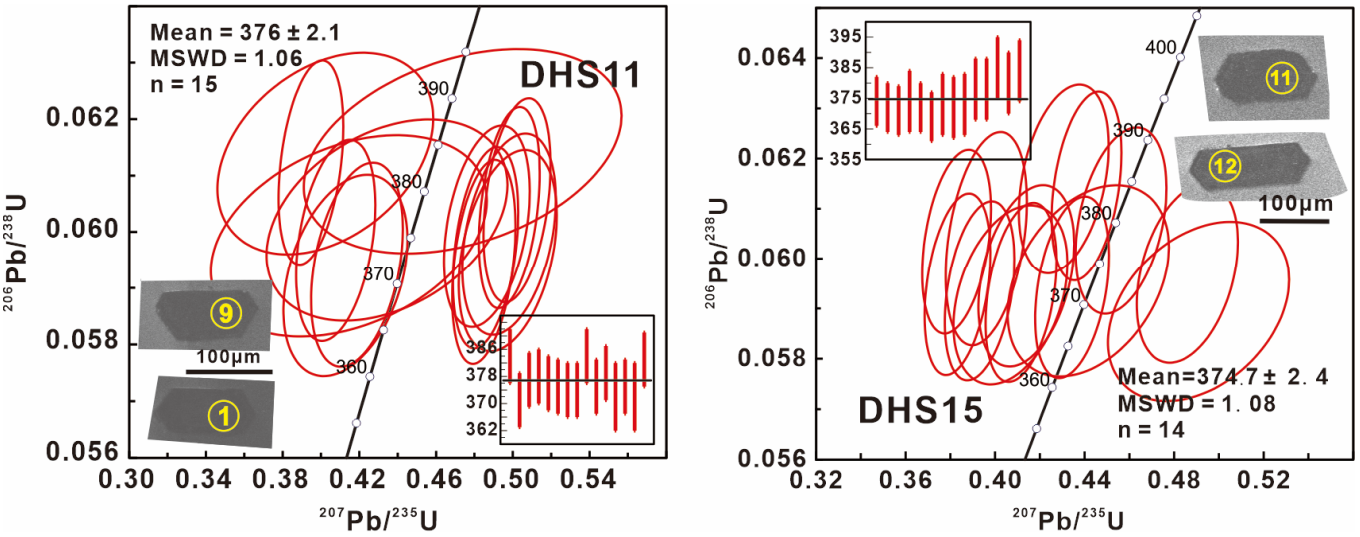

Figure 4. Concordia diagrams for samples DHS11 and DSH15 from the Duhongshan granites. Cathodoluminescence images for two zircons from each sample are also known.

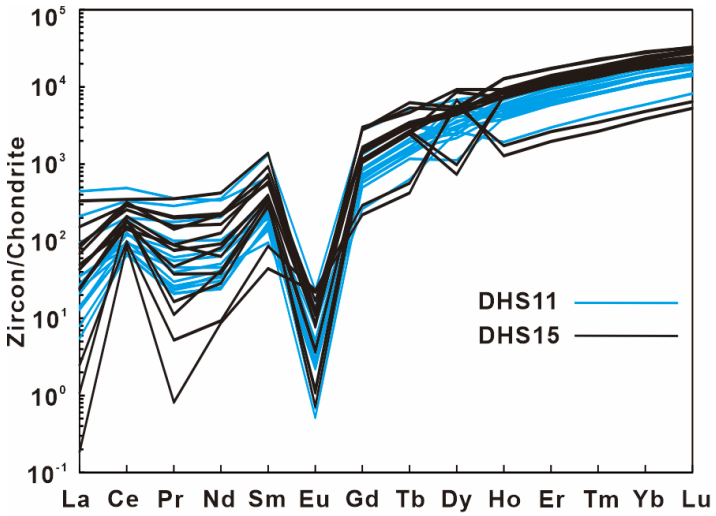

Figure 5. Chondrite−normalized rare earth element pattern for zircon from the Duhongshan granites. Chondrite values from [60].

4.2. Whole-Rock Major and Trace Elements

All analyzed samples from the Duhongshan pluton have low LOL values (0.40–1.09). They have high SiO_2 (68.3–73.3 wt.%), Al_2O_3 (13.1–14.9 wt.%), K_2O (6.6–7.2 wt.%), and Na_2O (4.6–5.5 wt.%) contents and K_2O/Na_2O ratios (1.1–1.6), as well as low P_2O_5 (0.01–0.30 wt.%), TiO_2 (0.05–0.35 wt.%), MgO (0.04–0.33 wt.%), and $Mg^{\#}$ (Mg# = 100 × $Mg^{2+}/(Mg^{2+} + Fe^{2+})$

values (5–26). In the SiO_2-versus-K_2O + Na_2O (TAS) diagram, the samples were plotted in the quartz monzogranite and granite field (Figure 6a). They belong to the shoshonite series in the SiO_2-versus-K_2O diagram (Figure 6b). All the samples are peralkaline in their compositions, with A/CNK (molar $Al_2O_3/(CaO + Na_2O + K_2O)$ ratios = 0.75 − 0.86) and A/NK (molar $Al_2O_3/(Na_2O + K_2O)$ ratios = 0.81 − 0.97) (Figure 6c). These geochemical features are similar to typical A-type granites [61].

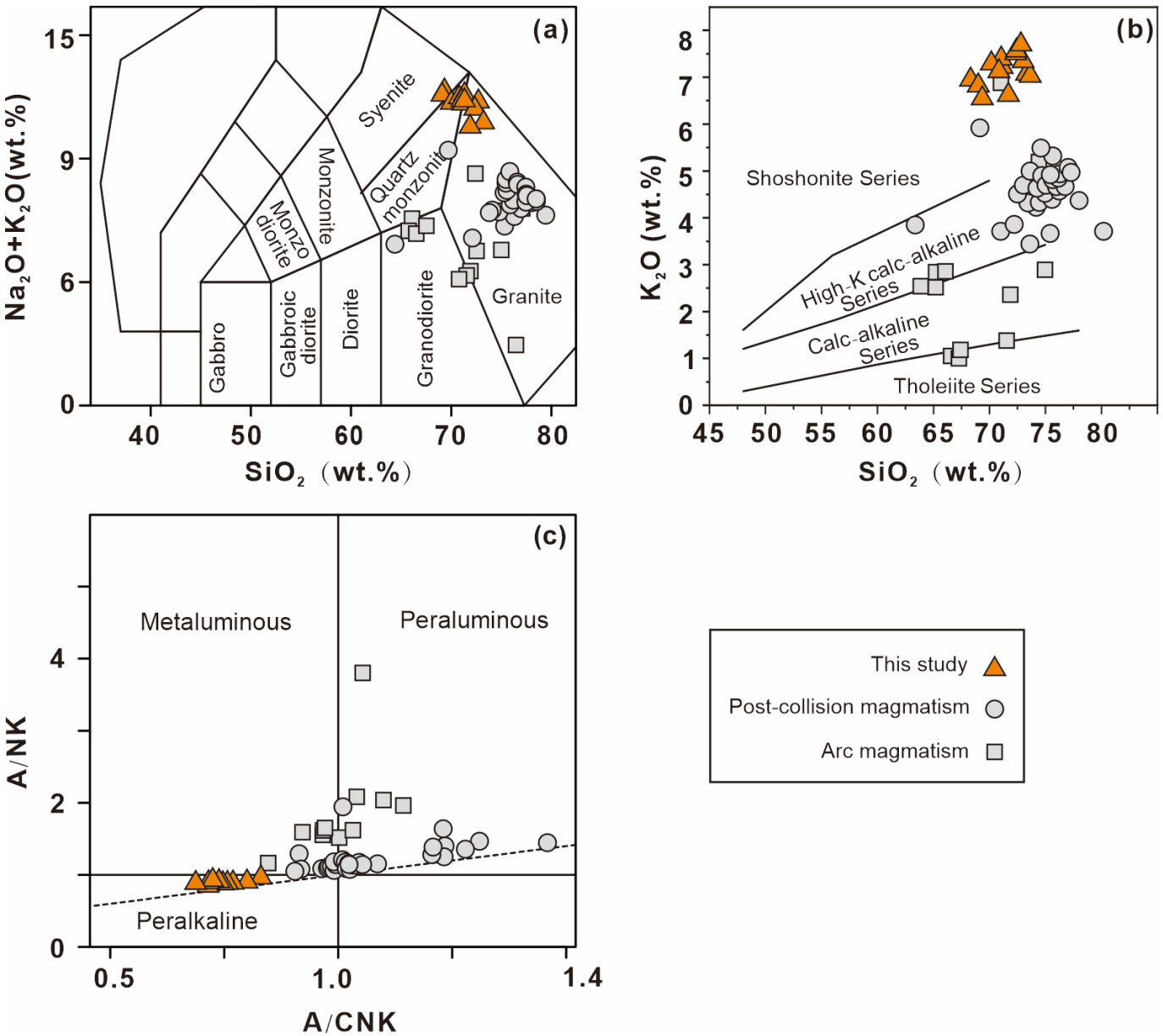

Figure 6. Major element diagrams for granitoids from the middle Huaniushan arc. (**a**) $Na_2O + K_2O$ vs. SiO_2 diagram [62]; (**b**) SiO_2 vs. K_2O diagram [63]; (**c**) A/NK vs. A/CNK diagram [64]. Geochemical data of post-collision and arc magmatism from [15,18,22–28].

The samples exhibit a high concentration of rare earth elements (REEs = 315–500 ppm), with a LREE/HREE ratio of 0.69–1.22. They are enriched in Rb, Th, K, and Pb and depleted in high field strength elements (HFSEs, e.g., Nb, Ta and Ti) as well as Ba, Sr, and P (Figure 7b), with significant Eu anomalies (δEu = 0.1) in the Chondrite-normalized REEs patterns (Figure 7a).

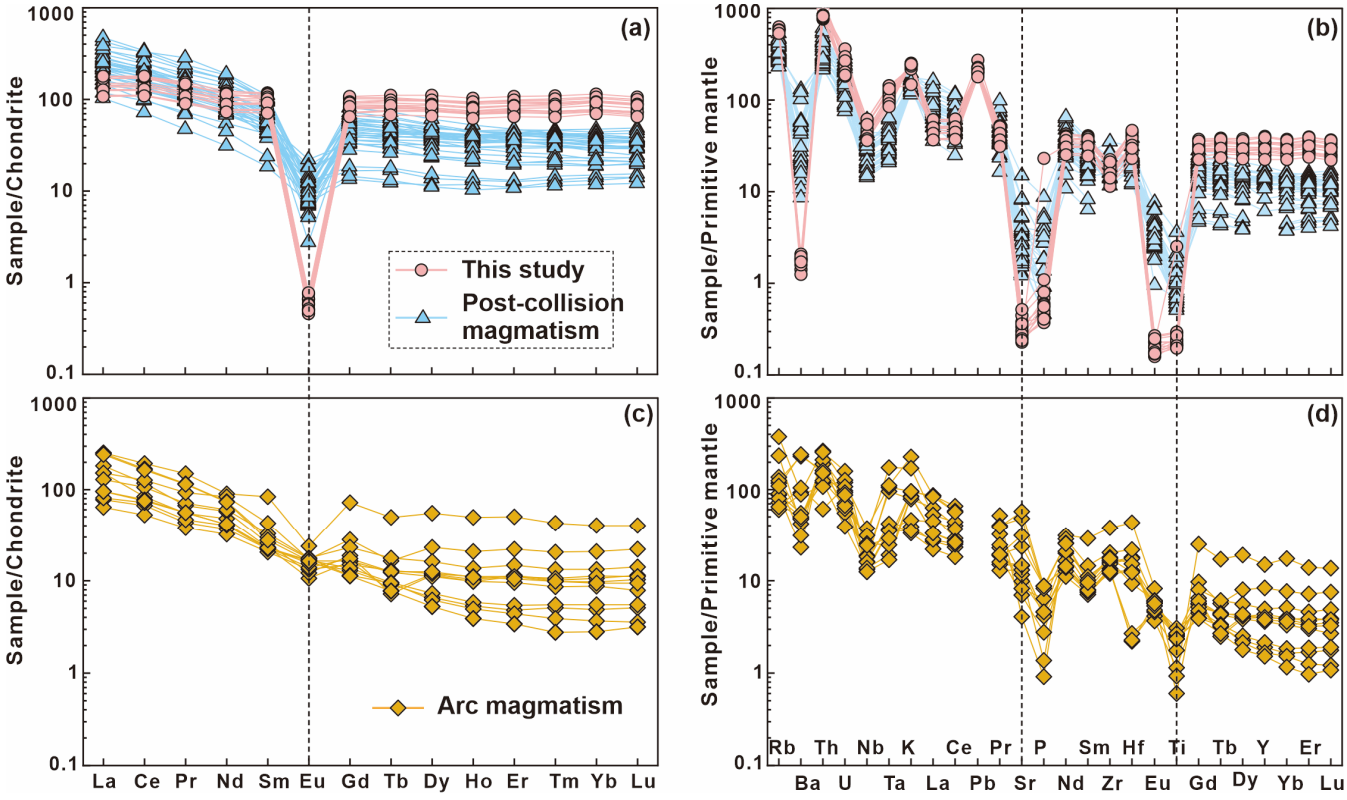

Figure 7. Chondrite-normalized rare earth element diagram (**a**,**c**) and primitive mantle-normalized trace elements diagram (**b**,**d**) for the granitoids from the middle Huaniushan arc. Chondrite and primitive mantle values from [60]. Geochemical data of post-collision and arc magmatism from [15,18,22–28].

4.3. Whole-Rock Nd Isotope

Initial Nd isotope ratios were calculated using the zircon U-Pb ages (374 Ma). The samples from the Duhongshan pluton have uniform measured $^{143}Nd/^{144}Nd$ ratios (0.512732–0.512753), which correspond to relatively constant initial $^{143}Nd/^{144}Nd$ ratios (0.512248–0.512267). They have positive $\varepsilon_{Nd}(t)$ values from +1.9 to +2.2 with two-stage Nd model ages (T_{DM2}) between 1.23 and 1.27 Ga (Table S4), which are older than zircon U-Pb crystallization ages.

5. Discussion

5.1. Early-Late Paleozoic Magmatism of Middle Huaniushan Arc

Intense magmatic activities occurred during the Late Paleozoic in the middle of the Huaniushan arc, with the reported LA-ICP-MS zircon U-Pb ages being centered in the range of 424–367 Ma (Figure 1c). The majority of the rocks are granitoids (SiO_2 > 63 wt.%), which include A- and I- type granites as well as adakites (Table 1). The rocks were divided into two groups based on their tectonic setting: post-collision [18,22–26] and active continental margin arc [28–30]. For A-type granites (Figure 8) belonging to the post-collision group, the zircon U-Pb ages range from 415 to 371 Ma. They exhibit the characteristics of high SiO_2 (63.4–80.2 wt.%) and K_2O (3.7–5.3 wt.%) [15,27,28], and all the samples plot into the granite field in the TAS diagram (Figure 6a) as well as into the high-K calc-alkaline series in the SiO_2-versus-K_2O diagram (Figure 6b), with are peraluminous to metaluminous (Figure 6c). These rocks are enriched in Rb, Th, K, and Pb and depleted in Ba, Sr, and Ti (Figure 7b), with significant Eu anomalies (Figure 7a), indicating that they were generated from partial melting of a relatively shallow crustal source. Furthermore, in the tectonic setting discrimination diagram (Figure 9), the samples plot into the plate granites zone. In contrast, the granites of the active continental margin arc are mostly I-type granites (Figure 8) and adakites, and their mineral compositions are rich in aluminum minerals [15,27,28]. They

display high SiO_2 contents (Figure 6a), mainly fall into the high K and calc-alkaline (Figure 6b) series, and were from metaluminous to peraluminous (Figure 6c). Moreover, these rocks exhibit high Sr/Y ratios (6.5 to 176) with no Sr or Eu anomalies (Figure 7a) and are depleted in Nb, Ta, and Ti (Figure 7b), suggesting that they were formed by juvenile crust melting in an active continental margin arc setting, falling in the volcanic arc granite category in Figure 9.

Table 1. Summary of petrological and ages for granitoids in the middle Huaniushan arc.

Location	Rocks Type	Method	Ages	Geodynamic Setting	References
Niujuanzi	A-type granite	LA-ICP-MS	371 Ma	post-collisional	[22]
Shuangfengshan	A-type granite	LA-ICP-MS	415 Ma	post-collisional	[18]
Huitongshan	I -type granite	LA-ICP-MS	397 Ma	post-collisional	[23]
Eatern Huitongshan	Monzogranite	LA-ICP-MS	397 Ma	post-collisional	[24]
Shijinpo	Monzogranite	LA-ICP-MS	380 Ma	post-collisional	[25]
Shijinpo	Granite	LA-ICP-MS	409 Ma	post-collisional	[26]
Shijinpo	Monzogranite	Rb-Sr	388–386 Ma	post-collisional	[26]
Niujuanzi	A-type granite	LA-ICP-MS	376–374 Ma	post-collisional	This study
Huangcaotan	Granite	LA-ICP-MS	394 Ma	active continental margin arc	[27]
Shuangfengshan	Monzogranite	LA-ICP-MS	367 Ma	active continental margin arc	[28]
Liuyuan	Adakite	LA-ICP-MS	424 Ma	active continental margin arc	[15]

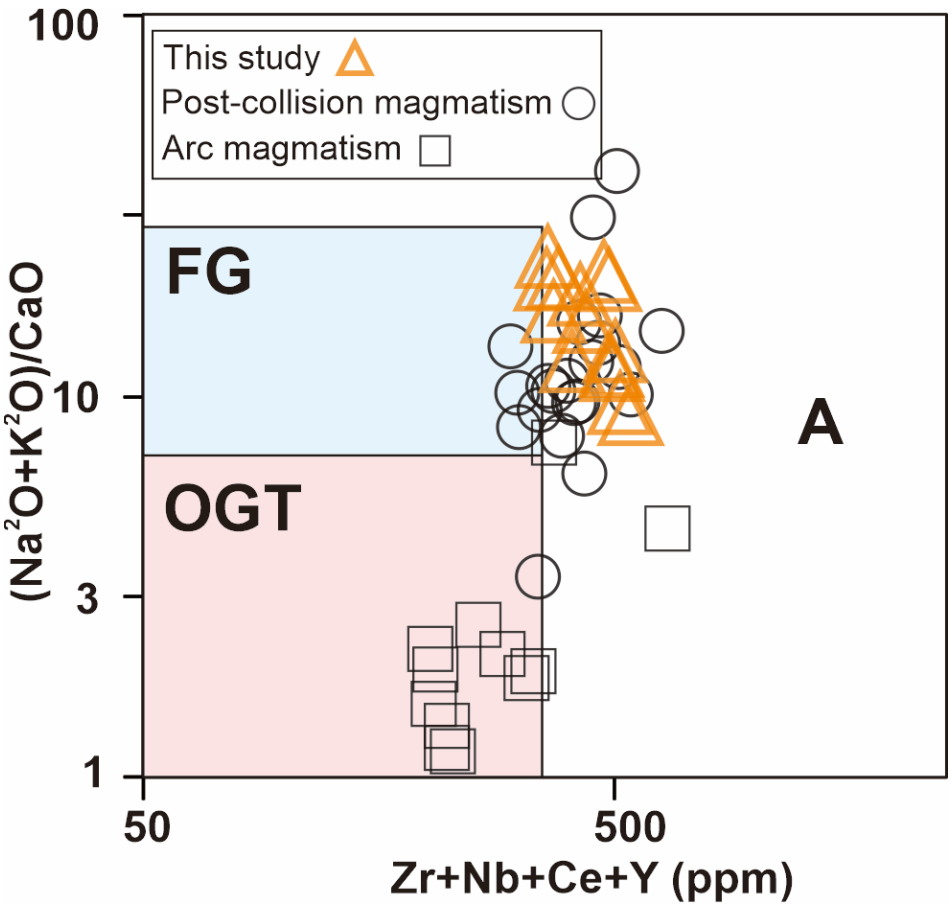

Figure 8. Discriminant diagram for type of granites from the middle Huaniushan arc in the BOB [61]. Geochemical data of post-collision and arc magmatism from [15,18,22–28]. FG = fractionated felsic granites; OGT = unfractionated I- and S-type granites; A = A-type granite.

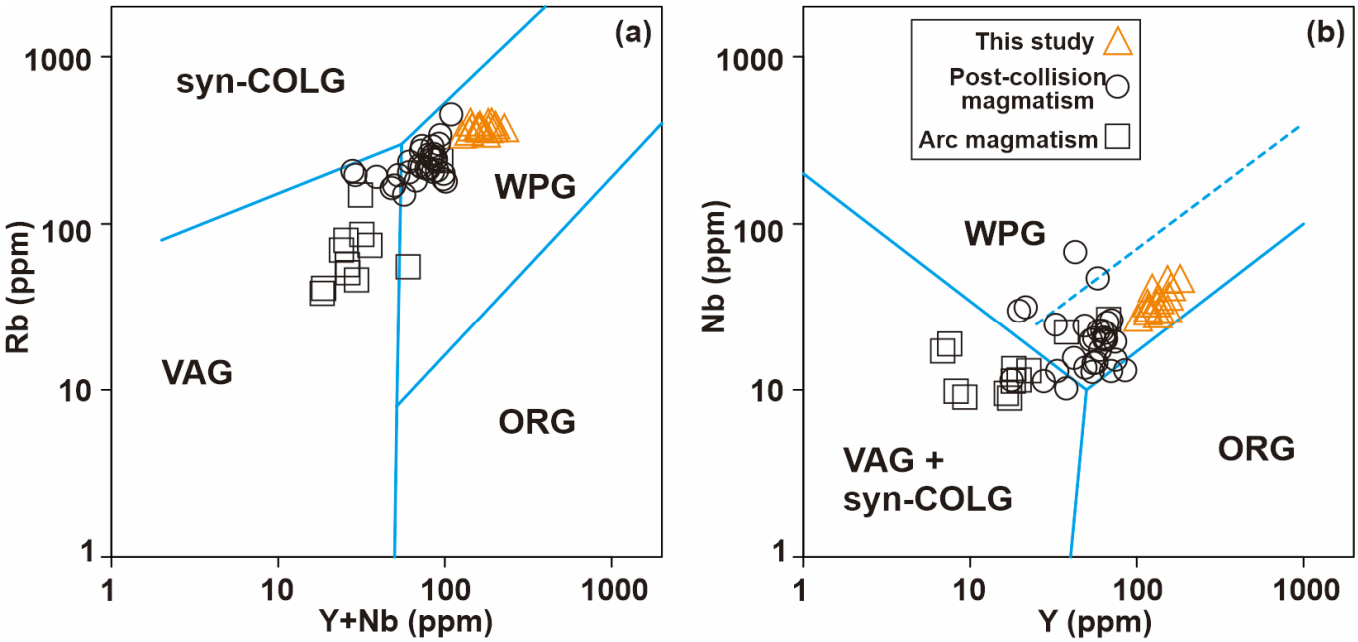

Figure 9. Geotectonic discrimination diagrams of granitoids from the middle of the Huaniushan arc. (**a**) Rb vs. Y + Nb diagram [65]; (**b**) Nb vs. Y diagram [65]. Geochemical data of post-collision and arc magmatism from [15,18,22–28]. Syn-COLG = syn collisional granite; VAG = volcanic arc granite; WPG = within-plate granite; POG = post-orogenic granite; ORG = oceanic ridge granite.

5.2. Petrogenesis of the Duhongshan Granites

Granites can be divided into S-, I-, M-, and A-types based on the geochemical and mineralogical features [66–69]. The Duhongshan granites have high K_2O (6.6–7.2 wt.%) contents, unlike M-type granites with low K_2O (<1 wt.%)., The Duhongshan granites have low A/CNK values (0.75–0.86) with contain no Al-rich minerals (e.g., garnet and andalusite), indicating the Duhongshan granites are not S-type granites. In addition, zircon saturation temperatures of the studied samples rang of 877–950 °C are higher than those of fractionated granites (average = 780 °C) [70], and majority samples plot in the A-type granite field rather than the field of fractionated felsic granites on the $(K_2O + Na_2O)/CaO$ vs. (Zr + Nb + Ce + Y) diagram (Figure 8). Thus, the Duhongshan granites are not highly fractionated granites.

However, remarkably, The Duhongshan granites have geochemical characteristics typical of A-type granites [64,68]. The studied sample rocks exhibit high SiO_2, low CaO and MgO contents, a K_2O/Na_2O ratio of 1.1–1.6, typical of the shoshonite features (Figure 6b), a 10,000 × Ga/Al value of 4.1–4.9 and a (Zr + Nb + Ce + Y) value of 354–543 ppm. It also exhibits a high Rb (341–397 ppm), and a high zircon saturation temperature [67] between 877 and 950 °C, much higher than the I- and S-type granites and consistent with A-type granites [68]. In addition, on the 10,000 × Ga/Al vs. (Zr + Nb + Ce + Y) diagram (Figure 10), the samples plot display a evolution trend of A-type granites, which are distinct from those of other granites. Therefore, these features indicate that the Duhongshan granites are belong to A-type granites.

Common works suggest that the A-type granites have three main petrogenetic mechanisms: (1) fractional crystallization of mantle-derived basaltic magmas [72]; (2) mixing of crust-derived granitic and mantle-derived mafic magmas [73]; and (3) partial melting of a crustal source [61,74]. There was not large-scale mafic magmatic co-occurrence in the middle Huaniushan arc (Figure 1c), and no find mafic xenoliths or other mantle-derived magma mixing phenomena from the Duhongshan granites, replying that the Duhongshan granites are not the result of mantle-derived basaltic magma separation crystallization. However, the Duhongshan granites did experience variable degrees of fractional crystallization. Such as the samples have negative Eu anomalies (Figure 7a), depletion in Ba, Nb,

Sr, P, Eu, and Ti (Figure 7b), low Ba (8.70–14.60) and Sr (4.67–10.67) contents, and low Zr/Hf (15.8–18.4) and Nb/Ta (6.7–8.0) ratios, suggesting fractionation of plagioclase and mafic and titanium-rich minerals [75,76].

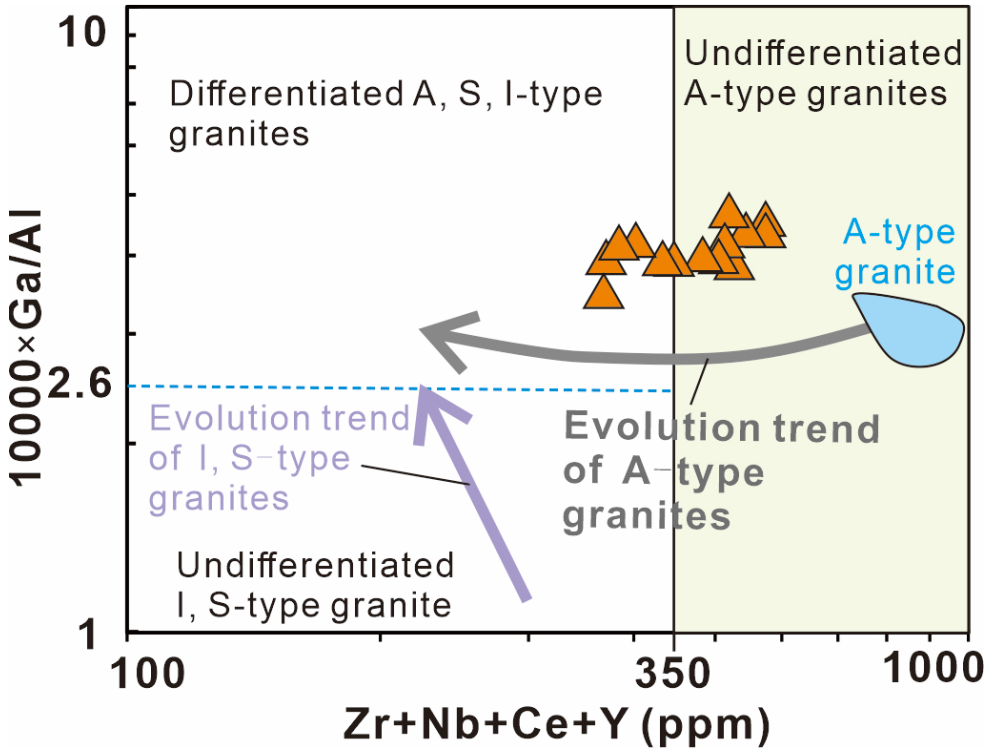

Figure 10. 10,000 × Ga/Al vs. (Zr + Nb + Ce + Y) diagram of the samples plot from the Duhongshan granites [71].

The Duhongshan granites display the same geochemical evolution trends as post-collision magmatism from the middle Huaniushan arc, such as Al_2O_3, CaO, Fe_2O_3, Na_2O, Ba, and Nb being negatively correlated with SiO_2 (Figure 11). They have higher K_2O and Na_2O than other granitoids with belong the shoshonite series (Figure 6b), indicating they are a late product of post-collision magmatism. The $Mg^{\#}$ values for partial melting magma is less than 45, whereas partial melts involving mantle material exceeds 45 [77], indicating that the Duhongshan granites ($Mg^{\#}$ values of 5–26) were derived from the partial melting of crustal material. Moreover, the Duhongshan granites are enriched in Th, U, and K (Figure 7b), and the Rb/Nb ratios (8.5–14.1) are close to the crustal value [60]. The Nb/Ta ratios are close to the lower crust value (8.3) [78], a good proxy that indicates that the studied samples are formed by the partial melting of crust-derived material. However otherwise, the studied samples have positive whole-rock $\varepsilon_{Nd}(t)$ values (1.87 to 2.20), indicating the source of the Duhongshan A-type granites add the mantle material. The two-stage Nd isotopic model ages (T_{DM2}) of the Duhongshan granites are in the range of 1226–1270 Ma. Therefore, these characteristics lead us to suggest that the Duhongshan A-type granites originated from the partial melting of the Mesoproterozoic lower crust material, with minor part from the mantle.

In conclusion, the Late Devonian A-type granites from the Duhongshan were generated from the heating by asthenosphere underplating subsequently resulted partial melting of the lower crust, and the underwent fractional crystallization.

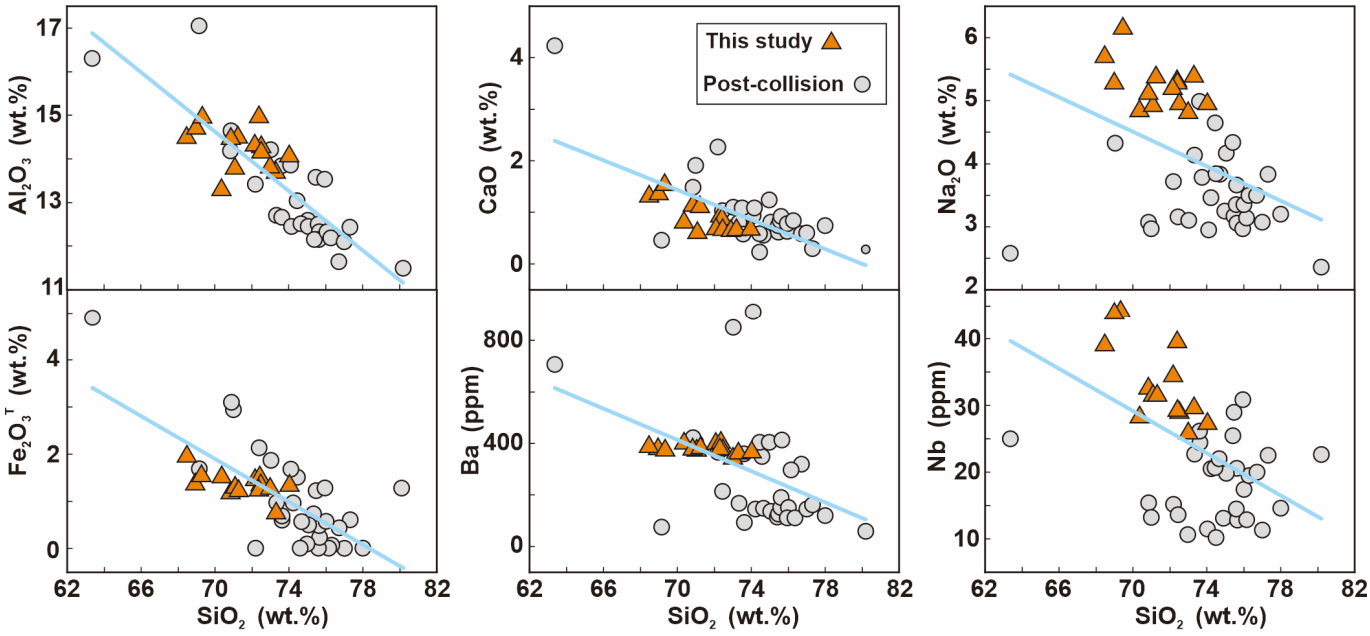

Figure 11. Harker diagrams for granitoids from the middle Huaniushan arc. Geochemical data of post-collision from [18,22–26].

5.3. Late Silurian-Devonian Magmatism Responses to Closure of PAO

The BOB comprises a complete record of the subduction, closure, and post-collision evolution history of the PAO during the Paleozoic–Mesozoic [11,33,34,37,79]. The 424–367 Ma magmatic activities are most widely distributed in the middle Huaniushan arc in the BOB and linked with ocean subduction and the continental collision of branch oceans of the PAO, and they are able to provide credible proof of the closure of the ocean [24,28]. The HNXO (Hongliuhe-Niujuanzi-Xichangjing ophiolite) is believed to be the earliest-subducted ocean (536–464 Ma) [32,39,40,80], and the ocean subduction was initiated in the Early Paleozoic. The subduction-related island arc-type magmatism developed in the Huaniushan arc and the Gongpoquan arc, which are believed to be the result of the southward subduction of the HNXO [17,28,31,40], accompanied by a series of brittle–ductile shearing deformation [6]. Additionally, this ocean continued to subduct during the Silurian, also supported by the Gongpoquan groups, resulting in a series of volcanic–sedimentary formations with felsic volcanic rocks in the island arc environments [54].

However, there is an abundance of geological evidence to support the theory that the HNXO began to close and collide during the Early Devonian. (a) SHRIMP dating of the cumulate gabbro, an important part of the Hongliuhe ophiolite, have provided a crystallization age from 520 Ma to 516 Ma, while the age of the undeformed biotite granites invading the Hongliuhe ophiolite is 404 Ma, and the SHRIMP zircon age of the undeformed granite overlying it is 413 Ma [30,80]. (b) The bedded limestone and silica-rich deposits in the central part of the BOB, which were produced in deep-sea environments during the Middle–Late Cambrian, are unconformably underlined by Devonian sedimentary rocks [57]. (c) Thick Devonian molassic deposits [53–56] and the large post-orogenic granite crop out in the Huaniushan arc (Figure 1c). These features suggest that the HNXO was closed in the Early Devonian. According to geochemical data (Y/Nb and Rb/Nb ratios) as well as tectonic information, the A-type granites can be further divided into A1-type in non-orogenic and A2-type in syn-collision or post-collision tectonic environments [66]. The Duhongshan granites exhibit high Y/Nb (3.2–5.3) and Rb/Nb (8.5–14.1) ratios and samples plot into the WPG field in Figure 9a,b, indicating they are A2-type granites formed in post-collision tectonic settings. They exhibit homogeneous geochemical characteristics for the granitoids in the middle Huaniushan arc, which were formed in post-collisional settings during the Silurian–Devonian (Figure 7a,b, Figures 8 and 9). Beyond that, the lower

Devonian stratigraphic strata of volcanic–sedimentary sequence in the southern part of the BOB indicate an extensional tectonic setting, distinct from the molassic deposits [11,38]. This indicates that the oceans closed during the Ordovician–Silurian, and that the region was an unstable environment. In the Late Devonian, this region entered the post-collisional extensional tectonic stage. During that period, the crust was thickened continuously due to the subduction and closure of the HNXO with occurred slab breakoff, and the lower crust was heated by the upwelling of asthenosphere magma, which resulted in the partial melting of the lower crust and developed the large-scale post-collisional magmatism in the Huaniushan arc.

In addition, the Late Silurian–Devonian magmatism of active continental margin arc is also wide distribution in the middle Huaniushan arc (Figures 1c and 9), and it is mainly present as calc-alkaline I-type granites and adakites formed by the melting of the subducting plate [17,28,37]. Middle Silurian to Devonian Liuyuan turbidite and adakite were formed by the subduction of the Liuyuan Ocean in the Huaniushan region [37,81]. The early Carboniferous Hongliuyuan formation in the south of the BOB is a main part of the volcanic arc, deposited in a sedimentary basin adjacent to the island arc [82]. This indicates that the Liuyuan Ocean continued northward subduction during the Early Carboniferous [31] and closure in the Late Permian to Early Triassic [46]. In conclusion, the magmatic activities of the active continental margin arc are the product of the northward subduction of the Liuyuan Ocean on the southern margin of the Paleo-Asian Ocean during the Late Paleozoic.

5.4. Devonian Tectonic Evolution of the Southern BOB

Combined with the reported data, we developed a tectonic evolution model for the Southern BOB, shown in Figure 12. At this time, the main tectonic units in the south of the BOB are the Gongpoquan arc, the Huaniushan arc (microcontinental block), the HNXO (Niujuanzi ophiolitic mélange), and the Liuyuan Ocean (Liuyuan accretive wedge). From the end of the Silurian to the Early Devonian, the HNXO underwent southward subduction and closed, and then evolved into the post-collision extensional tectonic stage, accompanied by magmatic activities of the post-collision of this area [18,22–26], then, the Liuyuan Ocean underwent northward subduction to the Huaniushan arc, forming a large amount of calc-alkaline felsic rocks in the active continental margin arc [15,27,28].

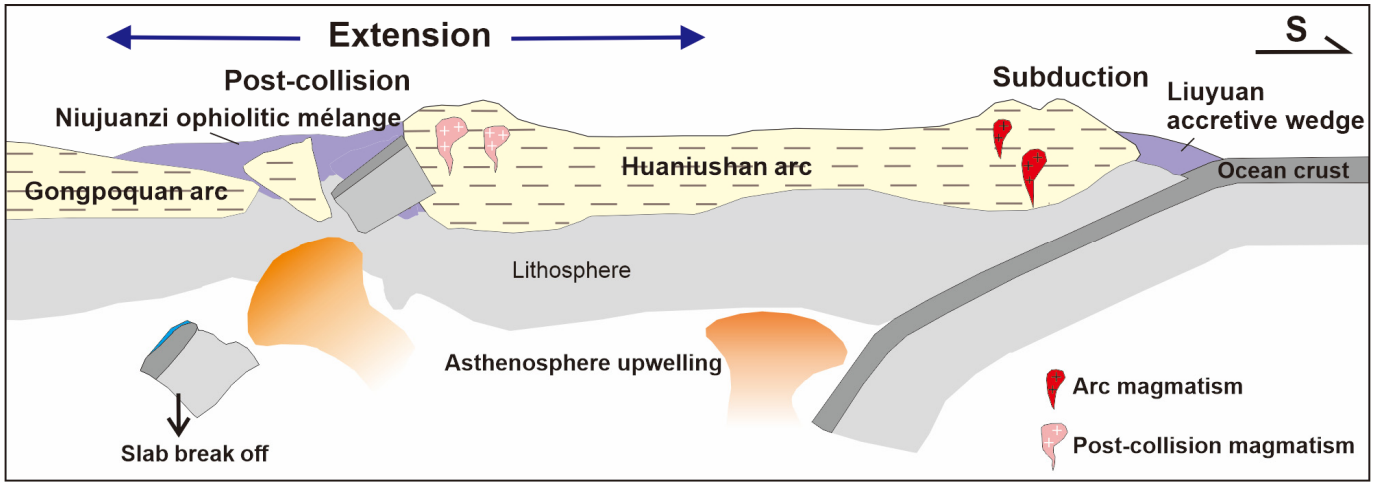

Figure 12. Simplified schematic model of the formation of Late Paleozoic granitoids from the middle Huaniushan arc and tectonic-magmatic evolution of the Southern Beishan Orogenic Belt.

6. Conclusions

A petrographic, geochronological, whole-rock major and trace element, and Nd isotopic study of Late Devonian granites in the BOB has led to the following conclusions.

(1) The LA-ICP-MS zircon U-Pb dating places the Duhongshan granites in the range of 376–374 Ma.
(2) The Duhongshan granites exhibit features of A2-type granites, suggesting that they were formed by partial melting of lower crustal material in post-collision extension settings.
(3) Combined with our new studies and previous regional investigations, we propose that the HNXO of the branch PAO closed during the Devonian.

Supplementary Materials: The following supporting information can be downloaded at: https://www.mdpi.com/article/10.3390/min13040565/s1, Table S1: Results of U-Pb dating by of zircons from the Duhongshan granites; Table S2: Zircon trace elements (ppm) analysis result of the Duhongshan granites; Table S3: Whole-rock major (wt.%) and trace element (ppm) analyses of the Duhongshan granites; Table S4: Whole-rock Nd isotopic data for the Duhongshan granites.

Author Contributions: Methodology, E.W., X.Z., W.C. and J.Z.; Investigation, E.W., W.C., L.W., G.S., Y.W. and Z.G.; Resources, E.W.; Data curation, E.W., W.C., L.W., G.S., Y.W. and Z.G.; Writing—original draft, E.W.; Writing—review and editing, X.Z., J.Z. and J.W.; Project administration, J.W.; Funding acquisition, X.Z. and J.W. All authors have read and agreed to the published version of the manuscript.

Funding: This research was supported by the China Atomic Energy Authority (CAEA) through the Geological Disposal Program and the National Second Expedition to the Tibetan Plateau (2019QZKK0901).

Data Availability Statement: The original contributions presented in the study are included in the article/Supplementary Material.

Acknowledgments: We would like to thank Conghui Xiong and Xiaoli Yan for their valuable help in test analysis. We sincerely thank the editors and all reviewers for their valuable feedback that we have used to improve the quality of our manuscript.

Conflicts of Interest: The authors declare no conflict of interest.

References

1. Şengör, A.M.C.; Natal'in, B.A.; Burtman, V.S. Evolution of the Altaid tectonic collage and Palaeozoic crutal growth in Eurasia. *Nature* **1993**, *364*, 299–307. [CrossRef]
2. Jahn, B.-M.; Wu, F.; Chen, B. Granitoids of the Central Asian Orogenic Belt and continental growth in the Phanerozoic. *Earth Environ. Sci. Trans. R. Soc. Edinb.* **2000**, *91*, 181–193. [CrossRef]
3. Xiao, W.J.; Windley, B.F.; Huang, B.C.; Han, C.M.; Yuan, C.; Chen, H.L.; Sun, M.; Sun, S.; Li, J.L. End-Permian to mid-Triassic termination of the accretionary processes of the southern Altaids: Implications for the geodynamic evolution, Phanerozoic continental growth, and metallogeny of Central Asia. *Int. J. Earth Sci.* **2009**, *98*, 1189–1217. [CrossRef]
4. Xiao, W.J.; Song, D.F.; Windley, B.F.; Li, J.L.; Han, C.M.; Wan, B.; Zhang, J.E.; Ao, S.J.; Zhang, Z.Y. Research progresses of accretion and metallogenies of the Central Asian Orogenic Belt. *Sci. China Earth Sci.* **2019**, *49*, 1512–1545, (In Chinese with English abstract). [CrossRef]
5. Yang, G.; Li, Y.; Tong, L.; Wang, Z.; Si, G. An Early Cambrian plume-induced subduction initiation event within the Junggar Ocean: Insights from ophiolitic mélanges, arc magmatism, and metamorphic rocks. *Gondwana Res.* **2020**, *88*, 45–66. [CrossRef]
6. Ao, S.J.; Xiao, W.J.; Han, C.M.; Li, X.H.; Qu, J.F.; Zhang, J.E.; Guo, Q.Q.; Tian, Z.H. Cambrian to early Silurian ophiolite and accretionary processes in the Beishan collage, NW China: Implications for the architecture of the Southern Altaids. *Geol. Mag.* **2012**, *149*, 606–625. [CrossRef]
7. Su, B.-X.; Qin, K.-Z.; Zhou, M.-F.; Sakyi, P.A.; Thakurta, J.; Tang, D.-M.; Liu, P.-P.; Xiao, Q.-H.; Sun, H. Petrological, geochemical and geochronological constraints on the origin of the Xiadong Ural–Alaskan type complex in NW China and tectonic implication for the evolution of southern Central Asian Orogenic Belt. *Lithos* **2014**, *200–201*, 226–240. [CrossRef]
8. Ren, R.; Han, B.-F.; Xu, Z.; Zhou, Y.-Z.; Liu, B.; Zhang, L.; Chen, J.-F.; Su, L.; Li, J.; Li, X.-H.; et al. When did the subduction first initiate in the southern Paleo-Asian Ocean: New constraints from a Cambrian intra-oceanic arc system in West Junggar, NW China. *Earth Planet. Sci. Lett.* **2014**, *388*, 222–236. [CrossRef]
9. Liu, Q.; Zhao, G.; Han, Y.; Zhu, Y.; Wang, B.; Eizenhöfer, P.R.; Zhang, X. Detrital zircon provenance constraints on the final closure of the middle segment of the Paleo-Asian Ocean. *Gondwana Res.* **2019**, *69*, 73–88. [CrossRef]

10. Bu, J.J.; He, W.H.; Zhang, K.X.; Yu, Y.; Wang, J.X.; Wu, J. Evolution of the Paleo-Asian Ocean: Evidences from Paleontology and Stratigraphy. *Earth Sci.-J. China Univ. Geosci.* **2020**, *45*, 711–727. [CrossRef]
11. Niu, Y.-Z.; Shi, G.R.; Ji, W.-H.; Zhou, J.-L.; Wang, J.-Q.; Wang, K.; Bai, J.-K.; Yang, B. Paleogeographic evolution of a Carboniferous–Permian sea in the southernmost part of the Central Asian Orogenic Belt, NW China: Evidence from microfacies, provenance and paleobiogeography. *Earth-Sci. Rev.* **2021**, *220*, 103738. [CrossRef]
12. Li, J.; Liu, J.; Wang, Y.; Zhu, D.-C.; Wu, C. Late Carboniferous to Early Permian ridge subduction identified in the southeastern Central Asian Orogenic Belt: Implications for the architecture and growth of continental crust in accretionary orogens. *Lithos* **2021**, *384–385*, 105969. [CrossRef]
13. Ao, S.; Xiao, W.; Windley, B.F.; Mao, Q.; Han, C.; Zhang, J.E.; Yang, L.; Geng, J. Paleozoic accretionary orogenesis in the eastern Beishan orogen: Constraints from zircon U–Pb and 40Ar/39Ar geochronology. *Gondwana Res.* **2016**, *30*, 224–235. [CrossRef]
14. Wang, E.-T.; Zhai, X.-W.; Chen, W.-F.; Ma, Z.; Wu, L.; Guo, Z.-A.; Wang, Y.; Song, G.-R.; Wang, J.-R. Late Paleozoic tectonics of Southern Central Asian orogenic belt: Evidence from magmatic rocks in the northern Alxa, Northwest China. *Front. Earth Sci.* **2023**, *10*, 1046122. [CrossRef]
15. Mao, Q.G.; Xiao, W.J.; Han, C.M.; Sun, M.; Yuan, C.; Zhang, J.E.; Ao, S.J.; Li, J.L. Discovery of Middle Silurian adakite granite and its tectonic significance in LIuyuan area, Beishan Moutains, NW China. *Acta Petrol. Sin.* **2010**, *26*, 584–596, (In Chinese with English abstract).
16. Gao, R.; Xiao, L.; Pirajno, F.; Wang, G.-C.; He, X.-X.; Yang, G.; Yan, S.-W. Carboniferous–Permian extensive magmatism in the West Junggar, Xinjiang, northwestern China: Its geochemistry, geochronology, and petrogenesis. *Lithos* **2014**, *204*, 125–143. [CrossRef]
17. Wang, X.; Yuan, C.; Zhang, Y.; Long, X.; Sun, M.; Wang, L.; Soldner, J.; Lin, Z. S-type granite from the Gongpoquan arc in the Beishan Orogenic Collage, southern Altaids: Implications for the tectonic transition. *J. Asian Earth Sci.* **2018**, *153*, 206–222. [CrossRef]
18. Li, S.C.; Wang, H.T.; Li, G.; Wang, X.A.; Yang, X.P.; Zhao, Z.R. Zircon U-Pb age, origin and its tectonic significances of Huitongshan Devonian K-feldspar granites from Beishan orogen. *NW China Acta Petrol. Sin.* **2020**, *27*, 3055–3070, (In Chinese with English abstract).
19. He, X.; Fang, T.; Yang, Z.; Du, H.; Liu, H.; Wang, J.; Jia, R.; Zheng, W. Petrogenesis and tectonic implications of A-type granitoids in the Xingxingxia-Hongliujing Area, Eastern Tianshan. *Earth Sci.* **2022**, 1–26, (In Chinese with English abstract).
20. Xiao, W.; Qigui, M.; Windley, B.; Han, C.; Qu, J.; Zhang, J.; Ao, S.; Guo, Q.; Cleven, N.; Lin, S.; et al. Paleozoic multiple accretionary and collisional processes of the Beishan orogenic collage. *Am. J. Sci.* **2010**, *310*, 1553–1594. [CrossRef]
21. Li, S.; Wang, T.; Wilde, S.A.; Tong, Y.; Hong, D.; Guo, Q. Geochronology, petrogenesis and tectonic implications of Triassic granitoids from Beishan, NW China. *Lithos* **2012**, *134–135*, 123–145. [CrossRef]
22. Ji, B.; Yu, J.; Guo, L.; Guo, L.; Bu, T. Geochemistry characteristics and tectonic significance of the hearteerdele granite mass in middle Devonian in Beishan, Gansu. *J. Geomech.* **2017**, *23*, 357–368, (In Chinese with English abstract).
23. Li, S.; Wang, T.; Dong, Y.; Hong, D.; Ou, Z. Identification of the Early Devonian Shuangfengshan A-type granites in Liuyuan area of Beishan and its implications to tectonic evolution. *Acta Petrol. Mineral.* **2009**, *28*, 407–422, (In Chinese with English abstract).
24. Zhao, Z.; Guo, Z.; Wang, Y. Geochronogy, geochemical charateristics and tectonic implications of the granitoids from Liuyuan area, Beishan, Gansu province, northwest China. *Acta Petrol. Sin.* **2007**, *23*, 1847–1860, (In Chinese with English abstract).
25. Tian, Z. Study on the features and auriferous potentiality of Shijinpo rock body in Beishan mountain, Gansu province. *J. Xian Coll. Geol.* **1993**, *15*, 62–68, (In Chinese with English abstract). [CrossRef]
26. An, G. Characteristics of Shijinpo granites and their relationship to gold metallogenesis in the Beishan mountains, Northwestern Gansu. *Gansu Geol.* **2007**, *16*, 19–25, (In Chinese with English abstract).
27. Wang, J.; Dong, Y.; Zeng, Z.; Yang, G.; Sun, S.; Zhang, F.; Zhou, B.; Sun, J. Geochronology Geochemistry and Geological Significance of the Huangcaotan Pluton in the Southern Beishan Orogenic Belt. *Geoscience* **2016**, *30*, 937–949, (In Chinese with English abstract).
28. Lyu, X.; Yu, X.; Du, Z.; Kang, K.; Du, L.; Wang, C. Late Devonian magmatic event in the South Beishan orogenic belt, Gansu: Constraints from zircon U-Pb chronology, geochemistry and Sr-Nd-Hf isotopes. *Acta Petrol. Sin.* **2022**, *38*, 693–712, (In Chinese with English abstract). [CrossRef]
29. Zuo, G.; Zhang, S.; He, G.; Zhang, Y. Plate tectonic characteristics during the early paleozoic in Beishan near the Sino-Mongolian border region, China. *Tectonophysics* **1991**, *188*, 385–392. [CrossRef]
30. Cleven, N.; Lin, S.; Guilmette, C.; Xiao, W.; Davis, B. Petrogenesis and implications for tectonic setting of Cambrian suprasubduction-zone ophiolitic rocks in the central Beishan orogenic collage, Northwest China. *J. Asian Earth Sci.* **2015**, *113*, 369–390. [CrossRef]
31. Guo, Q.-Q.; Chung, S.-L.; Xiao, W.-J.; Hou, Q.-L.; Li, S. Petrogenesis and tectonic implications of Late Devonian arc volcanic rocks in southern Beishan orogen, NW China: Geochemical and Nd–Sr–Hf isotopic constraints. *Lithos* **2017**, *278–281*, 84–96. [CrossRef]
32. Shi, Y.; Zhang, W.; Kröner, A.; Li, L.; Jian, P. Cambrian ophiolite complexes in the Beishan area, China, southern margin of the Central Asian Orogenic Belt. *J. Asian Earth Sci.* **2018**, *153*, 193–205. [CrossRef]
33. Song, D.; Xiao, W.; Windley, B.; Qigui, M.; Ao, S.; Wang, H.; Li, R. Closure of the Paleo-Asian Ocean in the Middle-Late Triassic (Ladinian-Carnian): Evidence From Provenance Analysis of Retroarc Sediments. *Geophys. Res. Lett.* **2021**, *48*, e2021GL094276. [CrossRef]

34. Wang, E.; Wu, L.; Zhai, X.; Chen, W.; Su, R.; Guo, Z.; Wang, Y.; Wang, J. Geochronology, Petro-genesis and Tectonic Implications of Huaniushan Diorite Porphyrite from the Gansu Beishan Area in the Southern Central Asian Orogenic Belt. *Earth Sci.* **2022**, *47*, 3285–3300, (In Chinese with English abstract). [CrossRef]
35. Zhang, W.; Wu, T.; Zheng, R.; Feng, J.; Luo, H.; He, Y.; Xu, C. Post-collisional Southeastern Beishan granites: Geochemistry, geochronology, Sr–Nd–Hf isotopes and their implications for tectonic evolution. *J. Asian Earth Sci.* **2012**, *58*, 51–63. [CrossRef]
36. Zheng, R.; Wu, T.; Zhang, W.; Meng, Q.; Zhang, Z. Geochronology and geochemistry of late Paleozoic magmatic rocks in the Yinwaxia area, Beishan: Implications for rift magmatism in the southern Central Asian Orogenic Belt. *J. Asian Earth Sci.* **2014**, *91*, 39–55. [CrossRef]
37. Yu, J.; Guo, L.; Li, J.; Li, Y.; Smithies, R.H.; Wingate, M.T.D.; Meng, Y.; Chen, S. The petrogenesis of sodic granites in the Niujuanzi area and constraints on the Paleozoic tectonic evolution of the Beishan region, NW China. *Lithos* **2016**, *256–257*, 250–268. [CrossRef]
38. Niu, Y.; Liu, C.; Shi, G.R.; Lu, J.; Xu, W.; Shi, J. Unconformity-bounded Upper Paleozoic megasequences in the Beishan Region (NW China) and implications for the timing of the Paleo-Asian Ocean closure. *J. Asian Earth Sci.* **2018**, *167*, 11–32. [CrossRef]
39. Tian, Z.; Xiao, W.; Windley, B.F.; Lin, L.n.; Han, C.; Zhang, J.e.; Wan, B.; Ao, S.; Song, D.; Feng, J. Structure, age, and tectonic development of the Huoshishan–Niujuanzi ophiolitic mélange, Beishan, southernmost Altaids. *Gondwana Res.* **2014**, *25*, 820–841. [CrossRef]
40. Wang, H.T. Tectono-Magmatism and its Geological Significance in The Beishan Area of The Southern Part of the Central Asian Orogenic Belt. Ph.D. Thesis, Lanzhou University, Lanzhou, China, 2019. Volume 155 (In Chinese with English abstract).
41. Han, B.; He, G.; Wu, T.; Li, H. zircon u-pb dating and geochemical features of early paleozoic granites from tianshan, xinjiang: Implications for tectonic evolution. *Xinjiang Geol.* **2004**, *22*, 4–11, (In Chinese with English abstract).
42. Kozlovsky, A.M.; Yarmolyuk, V.V.; Salnikova, E.B.; Travin, A.V.; Kotov, A.B.; Plotkina, J.V.; Kudryashova, E.A.; Savatenkov, V.M. Late Paleozoic anorogenic magmatism of the Gobi Altai (SW Mongolia): Tectonic position, geochronology and correlation with igneous activity of the Central Asian Orogenic Belt. *J. Asian Earth Sci.* **2015**, *113*, 524–541. [CrossRef]
43. Liu, X.; Chen, B.; Jahn, B.-M.; Wu, G.; Liu, Y. Early Paleozoic (ca. 465 Ma) eclogites from Beishan (NW China) and their bearing on the tectonic evolution of the southern Central Asian Orogenic Belt. *J. Asian Earth Sci.* **2011**, *42*, 715–731. [CrossRef]
44. He, Z.-Y.; Klemd, R.; Yan, L.-L.; Zhang, Z.-M. The origin and crustal evolution of microcontinents in the Beishan orogen of the southern Central Asian Orogenic Belt. *Earth-Sci. Rev.* **2018**, *185*, 1–14. [CrossRef]
45. Yuan, Y.; Zong, K.; He, Z.; Klemd, R.; Jiang, H.; Zhang, W.; Liu, Y.; Hu, Z.; Zhang, Z. Geochemical evidence for Paleozoic crustal growth and tectonic conversion in the Northern Beishan Orogenic Belt, southern Central Asian Orogenic Belt. *Lithos* **2018**, *302–303*, 189–202. [CrossRef]
46. Wang, S.; Zhang, K.; Chen, F.; Wang, J.; Song, B.; Li, J.; Wang, W.; Dai, P. Recognition of a Permian to Triassic foreland basin in the central Beishan Orogen, NW China: Provenance variations and their constraints on latest Palaeozoic orogeny. *Palaeogeogr. Palaeoclimatol. Palaeoecol.* **2021**, *565*, 110168. [CrossRef]
47. Ma, B.; Qian, Z.; Keays, R.R.; Xu, G.; Duan, J.; Zhang, J.; Gao, W. Petrogenesis of the Permian Luotuoshan sulfide-bearing mafic-ultramafic intrusion, Beishan Orogenic Belt, NW China: Evidence from whole-rock Sr–Nd–Pb and zircon Hf isotopic geochemistry. *J. Geochem. Explor.* **2022**, *233*, 106920. [CrossRef]
48. Ye, X.F.; Zong, K.; Zhang, Z.; He, Z.; Liu, Y.S.; Hu, Z.; Wang, W. Geochemistry of Neoproterozoic granite in Liuyuan area of southern Beishan Orogenic Belt and its geological significance. *Geol. Bull. China* **2013**, *32*, 307–317.
49. Yuan, Y.; Zong, K.; He, Z.; Klemd, R.; Liu, Y.; Hu, Z.; Guo, J.; Zhang, Z. Geochemical and geochronological evidence for a former early Neoproterozoic microcontinent in the South Beishan Orogenic Belt, southernmost Central Asian Orogenic Belt. *Precambrian Res.* **2015**, *266*, 409–424. [CrossRef]
50. Zong, K.; Klemd, R.; Yuan, Y.; He, Z.; Guo, J.; Shi, X.; Liu, Y.; Hu, Z.; Zhang, Z. The assembly of Rodinia: The correlation of early Neoproterozoic (ca. 900 Ma) high-grade metamorphism and continental arc formation in the southern Beishan Orogen, southern Central Asian Orogenic Belt (CAOB). *Precambrian Res.* **2017**, *290*, 32–48. [CrossRef]
51. Huang, B.; Wang, G.; Li, X.; Bu, T.; Dong, Z.; Zhu, T. Precambrian tectonic affinity of the Beishan Orogenic Belt: Constraints from Proterozoic metasedimentary rocks. *Precambrian Res.* **2022**, *376*, 106686. [CrossRef]
52. Wang, L.; Yang, J.; Wang, X.; Qi, Q.; Quan, S.; Li, W.; Ye, M.; Xie, Q.; Jiang, A. Zircon SHRIMP U-Pb age of Dashantounan basic ultrabasic intrusion complex in the Beishan Mountain, Gansu Province. *Acta Petrol. Mineral.* **2015**, *34*, 697–709, (In Chinese with English abstract). [CrossRef] [PubMed]
53. Zuo, G.; Liu, C.; Bai, W.; Feng, Y. Volcano-molasse geological structure and geochemical signature in Devonian period collision orogenic in Beishan, Gansu-Inmongolia. *Acta Geol. Gansu* **1995**, *4*, 35–43, (In Chinese with English abstract).
54. Yu, J.; Li, X.; Liang, J.; Jiang, X.; Wang, G.; Wu, P. Evolution of the geological structure in Beishan area across Gansu Province, Xinjiang antonomous region and Inner Mongolia autonomous region-constraints on the timing of opening and closing of the Beishan Paleozoic oceanic Basin. *Xinjiang Geol.* **2012**, *30*, 205–209, (In Chinese with English abstract).
55. Zhang, Y.; Yuan, C.; Sun, M.; Long, X.; Xia, X.; Wang, X.; Huang, Z. Permian doleritic dikes in the Beishan Orogenic Belt, NW China: Asthenosphere–lithosphere interaction in response to slab break-off. *Lithos* **2015**, *233*, 174–192. [CrossRef]
56. Weis, D.; Kieffer, B.; Maerschalk, C.M.; Barling, J.; de Jong, J.T.M.; Williams, G.A.; Hanano, D.; Pretorius, W.; Mattielli, N.; Scoates, J.S.; et al. High-precision isotopic characterization of USGS reference materials by TIMS and MC-ICP-MS. *Geochemistry* **2006**, *7*. [CrossRef]

57. Wu, Y.; Zheng, Y. Genetic mineralogy of zircon and its constraints on U-Pb dating interpretation. *Chin. Sci. Bull.* **2004**, *49*, 1589–1604. (In Chinese) [CrossRef]
58. Hoskin, P.W.O. Trace-element composition of hydrothermal zircon and the alteration of Hadean zircon from the Jack Hills, Australia. *Geochim. Cosmochim. Acta* **2005**, *69*, 637–648. [CrossRef]
59. Hoskin, P.W.O.; Schaltegger, U. The Composition of Zircon and Igneous and Metamorphic Petrogenesis. *Rev. Mineral. Geochem.* **2003**, *53*, 27–62. [CrossRef]
60. Sun, W.; McDonough, W. Chemical and isotopic systematics of oceanic basalts: Implications for mantle composition and processes. *Geol. Soc. Lond. Spec. Publ.* **1989**, *42*, 313–345. [CrossRef]
61. Whalen, J.B.; Currie, K.L.; Chappell, B.W. A-type granites: Geochemical characteristics, discrimination and petrogenesis. *Contrib. Mineral. Petrol.* **1987**, *95*, 407–419. [CrossRef]
62. Middlemost, E.A.K. Naming materials in the magma/igneous rock system. *Earth-Sci. Rev.* **1994**, *37*, 215–224. [CrossRef]
63. Le Maitre, R.W. *A Classification of Igneous Rocks and Glossary Terms, Recommendations of the International Union of Geological Sciences Subcommission on the Systematics of Igneous Rocks*; Blackwell Scientific Publications: Oxford, UK, 1989; pp. 1–193.
64. Maniar, P.D.; Piccoli, P.M. Tectonic discrimination of granitoids. *Geol. Soc. Am.Bull.* **1989**, *101*, 35–643. [CrossRef]
65. Pearce, J.; Harris, N.; Tindle, A. Trace Element Discrimination Diagrams for the Tectonic Interpretation of Granitic Rocks. *J. Petrol.* **1984**, *25*, 956–983. [CrossRef]
66. Eby, N. Chemical subdivision of the A-type granitoids: Petrogenetic and tectonic implications. *Geology* **1992**, *20*, 641–644. [CrossRef]
67. Watson, E.B.; Harrison, T.M. Zircon saturation revisited: Temperature and composition effects in a variety of crustal magma types. *Earth Planet. Sci. Lett.* **1983**, *64*, 295–304. [CrossRef]
68. King, P.L.; Chappell, B.W.; Allen, C.M.; White, A.J.R. Are A-type granites the high-temperature felsic granites? Evidence from fractionated granites of the Wangrah Suite. *Aust. J. Earth Sci.* **2001**, *48*, 501–514. [CrossRef]
69. Clemens, J.D. S-type granitic magmas—Petrogenetic issues, models and evidence. *Earth-Sci. Rev.* **2003**, *61*, 1–18. [CrossRef]
70. Song, Y.; Liu, X.; Xiao, W.; Gong, X.H.; Liu, X.; Xiao, Y.; Zhang, Z.; Liu, P. Tectonic evolution of circum-Rodinia subduction: Evidence from Neoproterozoic A-type granitic magmatism in the Central Tianshan Block, northwest China. *Precambrian Res.* **2023**, *387*, 106976. [CrossRef]
71. Feng, S.; Chen, W.; Wang, H.; Ling, H.; Zhao, C.; Chen, P. Identification and petrogenesis of highly differentiated A-type granite formed in the Late Mesozoic, Central Jiangxi Province. *Acta Geol. Sin.* **2020**, *94*, 1227–1247, (In Chinese with English abstract).
72. Simith, D.R.; Noblett, J.; Wobus, R.A.; Unruh, D.; Douglass, J.; Beane, R.; Davis, C.; Goldman, S.; Kay, G.; Gustavson, B.; et al. Petrology and geochemistry of late-stage intrusions of the A-type, mid-Proterozoic Pikes Peak batholith (Central Colorado, USA): Implications for petrogenetic models. *Precambr* **1999**, *98*, 271–305. [CrossRef]
73. Kemp, A.; Wormald, R.J.; Whitehouse, M.J.; Price, R.C. Hf isotopes in zircon reveal contrasting sources and crystallization histories for alkaline to peralkaline granites of Temora, southeastern Australia. *Geology* **2005**, *33*, 797–800. [CrossRef]
74. Collins, W.J.; Beams, S.D.; White, A.; Chappell, B.W. Nature and origin of A-type granites with particular reference to southeastern Australia. *Contrib. Mineral. Petrol.* **1982**, *80*, 189–200. [CrossRef]
75. Schiano, P.; Monzier, M.; Eissen, J.P.; Martin, H.; Koga, K.T. Simple mixing as the major control of the evolution of volcanic suites in the Ecuadorian Andes. *Contrib. Mineral. Petrol.* **2010**, *160*, 297–312. [CrossRef]
76. Wu, F.; Liu, X.; Ji, W.; Wang, J.; Yang, L. Highly fractionated granites: Recognition and research. *Sci. China (Earth Sci.)* **2017**, *60*, 1201–1219. [CrossRef]
77. Rapp, R.P.; Watson, E.B. Dehydration Melting of Metabasalt at 8–32 kbar: Implications for Continental Growth and Crust-Mantle Recycling. *J. Petrol.* **1995**, *36*, 891–931. [CrossRef]
78. Rudnick, R.L.; Gao, S. *Composition of the Continental Crust. Treatise on Geochemistry 3*; Elsevier–Pergamon: Oxford, UK, 2003; pp. 1–64. [CrossRef]
79. Song, D.; Xiao, W.; Han, C.; Li, J.; Qu, J.; Guo, Q.; Lin, L.; Wang, Z. Progressive accretionary tectonics of the Beishan orogenic collage, southern Altaids: Insights from zircon U–Pb and Hf isotopic data of high-grade complexes. *Precambrian Res.* **2013**, *227*, 368–388. [CrossRef]
80. Zhang, Y.; Guo, Z. Accurate Constraint on formation and emplacement age og Hongliuhe ophiolite, boundary region between Xinjiang and Gansu Provinces and iti tectonic implications. *Acta Petrol. Sin.* **2008**, *24*, 803–809, (In Chinese with English abstract).
81. Guo, Q.; Xiao, W.; Hou, Q.; Windley, B.F.; Han, C.; Tian, Z.; Song, D. Construction of Late Devonian Dundunshan arc in the Beishan orogen and its implication for tectonics of southern Central Asian Orogenic Belt. *Lithos* **2014**, *184–187*, 361–378. [CrossRef]
82. Chen, C.; Pan, Z.; Xiu, D.; Wei, W.; Zhang, J.; Zhang, H.; Wang, S.; Chang, Z.; Wang, R. Analysis on Sedimentary Period, Depositional Environment, and Provenance Tectonic Setting of Hongliuyuan Formation in Beishan Area. *Acta Sedimentol. Sin.* **2017**, *35*, 470–479, (In Chinese with English abstract).